



Research Paper

Highly reactive and stable nanoscale zero-valent iron prepared within vesicles and its high-performance removal of water pollutantsDongyang Shi^{a,b}, Xia Zhang^a, Jianji Wang^a, Jing Fan^{a,*}^a School of Environment, Henan Key Laboratory for Environmental Pollution Control, Key Laboratory for Yellow River and Huai River Water Environment and Pollution Control, Ministry of Education, Henan Normal University, Xinxiang, Henan 453007, PR China^b Henan Institute of Technology, Xinxiang, Henan 453003, PR China

ARTICLE INFO

Keywords:

Nanoscale zero-valent iron
Vesicles
Self-assembly
Reactivity
Stability

ABSTRACT

Nanoscale zero-valent iron particles have large specific surface area and high reaction activity, and have been increasingly used for the degradation of environmental contaminants. However, rapid aggregation and deactivation hinder their wide applications. In this work, nanoscale zero-valent iron (NZVI) particles were prepared in vesicles, which were formed by self-assembly of amphiphilic block copolymer poly(1-vinylpyrrolidone-co-vinylacetate) (PVV) in aqueous tetrahydrofuran medium, and characterized with the aid of XRD, FTIR, SEM-EDX, TEM, XPS and DLS techniques. It was found that the NZVI particles were well encapsulated in the vesicles, and they could be stored directly in the air as solids, but the dried NZVI particles could be easily released from the vesicles once they were put in water. These NZVI particles showed some unique features, such as uniform nanometer size distribution (from 70 to 100 nm), vesicle-like morphology, and good dispersion. Activity and stability of the NZVI in vesicles were examined by using Cr(VI) and nitrobenzene as the model pollutants, and compared with the bare NZVI particles synthesized with the same procedures but without PVV. A dramatic difference in activity and stability was observed for the two different NZVI particles. The NZVI in vesicles showed a good chemical stability in the air, and still maintained its high reactivity in water. Such excellent performance might be attributed to the encapsulation of the NZVI by vesicles, which could impede well the strong agglomeration of metal particles in water and prevent metal particles from being oxidized in the air.

1. Introduction

Over the past years, nanoscale zero-valent iron (NZVI) particles have attracted much attention in the control of environmental pollutants because of their large specific surface area, high reaction activity, and strong reductive power [1]. Indeed, NZVI particles are very effective for the removal of various wastewater contaminants, such as nitrite [2], selenite [3], organic dyes [4], aromatic halides [5], and heavy metals contaminants [6,7]. However, due to the strong van der Waals and magnetic attraction forces as well as strong reductive power, bare NZVI particles not only tend to agglomerate into larger particles in the micro- to milli-meter scale, but also can be oxidized easily in the air with sharp deterioration of activity, durability and efficiency, which greatly impedes their large-scale application in real-life conditions [8].

To solve these problems, some techniques have been developed to prepare stable and well-dispersed NZVI particles, such as surface coating of NZVI with surfactant, polyelectrolyte or nature biopolymer [9–11], and immobilization of NZVI on inorganic or organic supports [12–15]. However, it is still a challenge to simultaneously strike a

trade-off between chemical reactivity in water and stability in the air [16]. Most strategies for the NZVI coating and supporting cannot be used to control dispersion, nanometer distribution, structure and morphology of the particles, which will significantly affect their reactivity in practical application. In addition, owing to the high reaction activity of NZVI, the surface modified NZVI particles have to be protected by inert gas in the preparation and storage processes. This has to increase the complexity of preparation and the cost of operation in real applications.

In recent years, polymeric vesicles or micelles, prepared by self-assembly of amphiphilic block copolymers in selective solvents, have attracted particular interest because of their unique properties and potential application in the fields of pharmaceutical, medical and catalysis. In this context, a very promising strategy is the preparation of stable and active noble metal nanoparticles, such as Au or Pd nanoparticles, by the *in situ* reduction in the vesicles or micelles of amphiphilic block copolymers. Li et al. [17] reported a thermally responsive vesicle system that could be easily decorated with gold nanoparticles by simply mixing the polymer solution with a NaAuCl₄ solution at 50 °C.

* Corresponding author.

E-mail address: fanjing@htu.cn (J. Fan).

Mai et al. [18] described a general method for the incorporation of Au particles into the central portion of the vesicles to allow the particles to be preferentially localized in the central portion of the walls, and the nanoparticles were radially distributed in the vesicles. KlingelÖfer et al. [19] prepared palladium hybrid colloids consisting of palladium colloids in the core of amphiphilic block copolymer micelles, which showed a strong catalytic activity and stability in the Heck reaction. Jaramillo et al. [20] synthesized highly dispersed Au nanoparticles by block copolymer micelle encapsulation and observed their catalytic activity to electro-oxidation of CO. More recently, Lin et al. [21] prepared photosensitizer-loaded gold vesicles for integrated photodynamic cancer therapy by a novel theranostic platform based on photosensitizer-loaded plasmonic vesicular assemblies. However, to the best of our knowledge, there are no studies on the preparation and application of more active NZVI in vesicles or micelles.

In this study, poly(1-vinylpyrrolidone-co-vinylacetate) (PVV) was selected to form vesicles in aqueous tetrahydrofuran (THF) solution by self-assembly due to its amphiphilicity, low toxicity and biodegradability. Then for the first time, NZVI particles were prepared in the vesicular nanoreactors and used to degrade environmental pollutants. Thus, the objective of this study is three-fold: (i) To synthesize NZVI particles in PVV vesicles and the possible mechanism was also studied with the aid of various characterization techniques; (ii) To investigate the reactivity in water and the stability in the air of NZVI in vesicles using Cr(VI) as a model; and (iii) To use the synthesized NZVI in vesicles as reductant in the application of nitrobenzene degradation in simulated wastewater, where the reaction kinetics was studied by using the pseudo-second-order decay model and the time evolution, and the intermediate and final products were analyzed.

2. Experimental

2.1. Chemicals

Amphiphilic block copolymer poly(1-vinylpyrrolidone-co-vinylacetate) (PVV) (copolymer (C_6H_9NO)_n($C_4H_6O_2$)_m, 7:3 or 3:7; 50% in ethanol; molecular weight = 591.69) was purchased from Aldrich Chem. Co. Inc. Sodium borohydride ($NaBH_4$), tetrahydrofuran (THF, C_4H_8O), ferric chloride hexahydrate ($FeCl_3 \cdot 6H_2O$), nitrobenzene, and commercial micro-scale Fe powder were purchased from Tianjin Kemiou Chemical Reagent Co. All the chemicals used in this work were analytical grade reagents and all the solutions were prepared using deionized water.

2.2. Synthesis of the NZVI in vesicles

Aqueous THF is a well-known solvent for the preparation of various block copolymer vesicles. In the present study, this mixed solvent was also used in the preparation of PVV assembly. To prepare the vesicles, 0.5 g of PVV (PVP-co-PVA) block copolymer (7:3) and 50 mL of deionized water were mixed in a 250 mL three-necked flask at room temperature, and the solution was kept sealed with stoppers. Then the mixture was titrated by 100 mL of THF with a rate of 0.03 mL min⁻¹ under stirring. When the system became cloudy, the formation of vesicles was suggested. The stirring was continued for another 60 min after completion of the titration. For comparison, 0.5 g of PVV block copolymer (3:7) was mixed with 50 mL of THF within 250 mL three-necked flask at room temperature, and 75 mL of deionized water was then added into the flask through titration with the same rate of 0.03 mL min⁻¹.

As depicted in Scheme 1, the resulting solutions were mixed with $FeCl_3 \cdot 6H_2O$ powder at different Fe^{3+} concentrations, and the mixtures were stirred for 30 min to allow Fe^{3+} was bound to ester groups of vinylacetate by coordination. To each vesicle/ Fe^{3+} solution, $NaBH_4$ powder was added immediately with a molar ratio of $NaBH_4$ to Fe^{3+} at 5:1. As expected, the solution became black quickly with spilling of a lot

of bubbles and a quicksand-like mixture was formed. The black paste was separated from the mixture by a magnet and washed with aqueous THF (H_2O : THF = 1:2 (v/v)) three times, then dried in a vacuum oven at 60 °C overnight. In this way, PVV/NZVI particles with different Fe^0 contents were synthesized, which were denoted by PVV/NZVI (8:1), PVV/NZVI (4:1), PVV/NZVI (2:1), PVV/NZVI (1:2) and PVV/NZVI (1:4) respectively, according to the increased concentration of Fe^{3+} . As a control experiment, bare NZVI particles were also synthesized by the identical procedures, but no copolymer was added in this case.

2.3. Characterization of the NZVI in vesicles

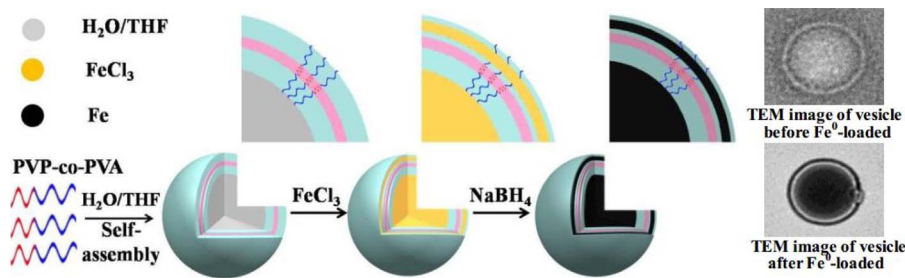
X-ray diffraction (XRD) spectra of NZVI in vesicles were recorded with a Bruker D8 Advance instrument (Germany) using K radiation over the 10–70° scan range. The elemental distribution analysis of the NZVI in vesicles was performed using an energy-dispersive X-ray (EDX) spectroscopy (Supra-40, Zeiss, Germany). Fourier transform infrared (FT-IR) spectra were recorded using a FTIR Analyzer (Perkin-Elmer, Spectrum 400, American) in the wavelength range of 4000–500 cm⁻¹, and the KBr was served as a reference. X-ray photoelectron spectroscopy (XPS) analysis was carried out using a Escalab 250Xi (UK) with a Al k X-ray (1486.7 eV). Surface charging effects were corrected with C 1s peak at 285 eV as a reference. Shirley baseline and a Gaussian-Lorentzian peak shape were used for fitting the data.

The microstructure and morphology of NZVI in vesicles were identified by transmission electron microscope (TEM, JEM-2100, Japan) with selected area electron diffraction (SAED) operated at 200 kV. The size distribution of NZVI in vesicles was calculated by visual particle counting with more than 100 particles. Dynamic light scattering (DLS) measurements were performed at 298.2 K by using a laser light scattering photometer (Nano-ZS90, Malvern, UK). Light of $\lambda = 633$ nm from a solid-state He-Ne laser (4.0 mW) was used as the incident beam. All measurements were made at 90° scattering angle and the intensity-average hydrodynamic diameter and particle dispersion index of the vesicles were calculated. All sample solutions were filtered through a 0.22 μm membrane filter.

2.4. Estimation of reactivity and stability

For the sake of convenience, the reactivity of PVV/NZVI particles was estimated by their ability to remove Cr(VI) from simulated wastewater. Typically, each of the seven iron sources including commercial micro-scale Fe powder (0.0022 g), bare NZVI (0.0026 g), PVV/NZVI (8:1, 0.045 g), PVV/NZVI (4:1, 0.030 g), PVV/NZVI (2:1, 0.020 g), PVV/NZVI (1:2, 0.005 g), PVV/NZVI (1:4, 0.003 g) were, respectively, added into a 50 mL conical flask containing 40 mL of aqueous Cr(VI) solution (initial pH = 5.6, and initial concentration $C_0 = 5 \text{ mg L}^{-1}$). In these procedures, the iron sources were used at the same iron content of 0.050 g L⁻¹. Besides, in the control experiment, pure block copolymer (0.045 g) was also used alone in a separate experiment. The Cr(VI) stock solution was deoxygenated by N_2 stream for 10 min before addition of iron sources and kept sealed with a stopper during the reaction. The removal experiment was carried out by putting the flask in a thermostatic shaker bath at 25 ± 0.5 °C for 100 min, with a rotation speed of 180 rpm. At the given time interval, 1 mL of solution was sampled and filtered through a 0.22 μm membrane. The Cr(VI) concentration was analyzed using the diphenylcarbohydrazide method [22]. The loading amount of NZVI was determined by the 1,10-phenanthroline colorimetric method [23]. The Cr(VI) concentration at time t ($C_t, \text{ mg L}^{-1}$) was determined, and the removal percent of Cr(VI) was calculated according to the equation: removal (%) = $(C_0 - C_t)/C_0 \times 100\%$. The experimental data of batch experiments were obtained in triplicate.

After the reduction of Cr(VI) by PVV/NZVI and bare NZVI, the solid samples were washed by deaerated ethanol twice with inert gas protection and were analyzed by XPS to test the composition of final



chromium products. Besides, the total concentration of chromium, i.e., $\text{Cr(VI)} + \text{Cr(III)}$, in the liquid samples was determined by oxidizing any trivalent chromium with potassium permanganate [24], followed by analysis as hexavalent chromium. The concentration of trivalent chromium was determined from the difference between total and hexavalent chromium. Furthermore, the pH value of the suspension during the reaction was also measured at different periods.

The stability of NZVI in vesicles was determined by evaluating its ability to remove Cr(VI) in water and examining XRD variation of the dried samples at different air exposure times. The experimental procedures for Cr(VI) removal and XRD characterization were the same as mentioned above.

2.5. Removal of nitrobenzene from aqueous solution

In order to simulate real application, all degradation experiments were performed without inert gas protection. For comparison, the removal of nitrobenzene with pure block copolymer and the bare NZVI particles were also investigated. A given amount of iron sources (containing 0.0020 g of Fe^0) was added into 40 mL of aqueous nitrobenzene solution ($\text{pH} = 6.0$, and initial concentration $C_0 = 12.5 \text{ mg L}^{-1}$). In addition, pure block copolymer alone was also used in a separate experiment, and its dosage was the same as that in PVV/NZVI (2:1). The reaction condition was similar to that for Cr(VI) removal. Sodium acetate buffer system was selected in this study to control pH of aqueous solution.

Nitrobenzene contents were determined using a Waters high performance liquid chromatography (HPLC) equipped with a reversed-phase column (C18 column, 4.6 mm × 250 mm). The mixture of methanol/water in the proportion of 60/40 was used as mobile phase at a flow rate of 1 mL min⁻¹. The injection volume was 20 μL and the detection wavelength was at 267 nm. The removal percent of nitrobenzene was calculated according to the above equation for Cr(VI) removal analysis. The data of batch experiments were also obtained in triplicates.

Scheme 1. Schematic illustration of the possible pathway for the formation of NZVI particles in the vesicles, where PVP and PVA of the copolymer (PVP-co-PVA) were marked by pink and glass blue, respectively. (For interpretation of the references to colour in this figure legend, the reader is referred to the web version of this article.)

3. Results and discussion

3.1. Synthesis of PVV vesicles and the NZVI in vesicles

3.1.1. Preparation of PVV vesicles in aqueous THF solution

It is known that the self-assembly of amphiphilic diblock copolymers in selective solvents generally results in micelles of a core-shell structure [25]. For the self-assembly of highly asymmetric amphiphilic diblock copolymers, such as PVP-co-PVA (7:3) and PVP-co-PVA (3:7), the resulting spherical micelle-like aggregates are usually prepared by dissolving the copolymers in a common solvent, and then a selective solvent, which is good for the short block, is added to the polymer solution. In the course of the self-assembly, the core is formed by insoluble long blocks while the shell is formed by soluble short blocks [26]. In this study, we selected two block ratios of the copolymer PVP-co-PVA (7:3 and 3:7) for possible preparation of the vesicles in aqueous THF solution. In doing so, the block copolymer PVP-co-PVA (7:3) was first dissolved in water and then THF was added to the polymer solution as a selective solvent for PVA. However, the block copolymer (3:7) was not soluble in water. Thus, this copolymer was first dissolved in THF and then water was added to the polymer solution as a selective solvent for PVP. Here, the property of the selective solvent and the long block (core forming block) plays a critical role in structure and morphology of the resulting aggregates. It has been reported that the solubility parameters (δ) of PVP, PVA, water and THF are 21.9, 20.7, 47.9 and 18.6 [M Pa]^{1/2} [27–29], respectively. This clearly indicates that the match of solubility parameters between selective solvent (THF) and long block PVP (core forming block) in the block copolymer PVP-co-PVA (7:3) was much closer than that between water and long block PVA (core forming block) in the block copolymer PVP-co-PVA (3:7). The closer the match between the solubility parameter of the selective solvent and that of the core forming block, the higher the degree of stretching of the core chains. As the degree of stretching of core forming chains in the cores increased, the structure of the aggregates could change progressively from micelles to vesicles [26]. Thus, the block copolymer PVP-co-PVA (7:3) tended to form vesicular aggregates, but PVP-co-PVA (3:7) generated micelles, which was well confirmed by TEM images of Fig. 1(A) and (B).

The image at lower magnification in Fig. 1(A) indicates that the as-

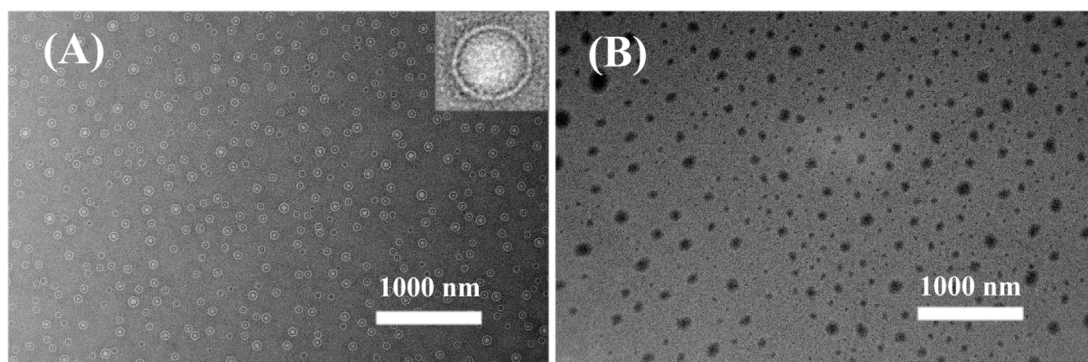


Fig. 1. TEM images of the aggregates formed by self-assembly of the PVV copolymer with block ratios of 7:3 (A) and 3:7 (B). Inset in (A) is the higher magnification image of aggregate.

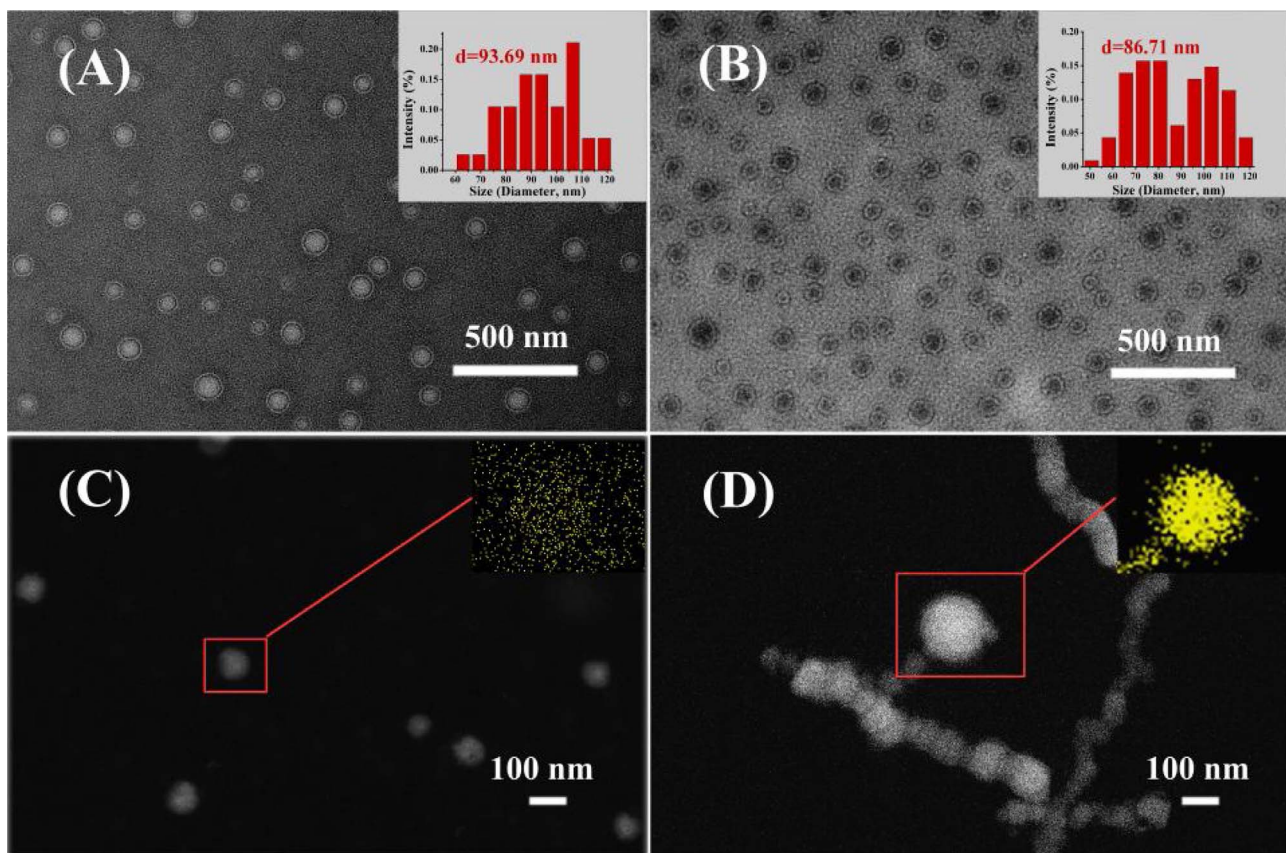


Fig. 2. TEM images and size distribution histogram (inset) of the vesicles before (A) and after (B) Fe^0 formation; SEM images of the NZVI in vesicles (C), bare NZVI (D) and their corresponding EDX elemental mapping images (inset).

prepared assembly by using the copolymer with block ratio of 7:3 was well-dispersed spherical vesicles and strikingly uniform in morphology. These vesicles showed a uniform nanometer size distribution from 70 to 100 nm. Moreover, it can be seen from the higher magnification image (inset in Fig. 1), the vesicle has a clear structural composition of wall and cavity, which not only offers protective shells for sensitive substances, but also provides containers where synthesis of the dispersed materials can be performed at the nanometer level. However, it can be seen from Fig. 1(B) that if the block ratio of the copolymer was 3:7, the as-prepared assembly was clumps of polymer particles and its nanometer distribution could not be controlled. In addition, it should be emphasized that no vesicles could be formed in water, which is crucial for the application of NZVI in vesicles in the removal of water pollutants. Therefore, the copolymer of PVV with block ratio of 7:3 and aqueous THF solution with volume ratio of 1:2 (H_2O : THF) were selected to prepare the PVV vesicles.

3.1.2. Preparation of the NZVI in the vesicles

Usually, the formation of metal nanostructure is highly dependent on the concentrations of the reagents [30]. To demonstrate the adjustability of the proposed synthetic route, the preparation of PVV/NZVI was performed as a function of Fe^{3+} concentration while the contents of the block copolymer and water/THF were kept constant. TEM images for PVV/NZVI with varied molar ratios were shown in Fig. S1 (see electronic supplementary information). It can be seen from Fig. S1 (A)–(C) that well-dispersed PVV/NZVI with similar spherical vesicle morphology had been obtained at the molar ratio of 8:1, 4:1 and 2:1. When the molar ratio of $-\text{COOC}-$ to Fe^{3+} was 8:1, a large number of blank vesicles coexisted with NZVI in the vesicles owing to high copolymer content. Fig. S1 (D) and (E) indicates that when the content of Fe^{3+} exceeded that of $-\text{COOC}-$, the synthesized nanoparticles were irregular because the amount of free Fe^{3+} ions in the solution was too

high to be encapsulated completely in the vesicles, resulting in the agglomeration of NZVI particles when Fe^{3+} was reduced to Fe^0 .

Fig. S2 shows the XRD pattern of the NZVI in vesicles prepared with molar ratios of $-\text{COOC}-$ to Fe^{3+} varying from 8:1 to 1:4. Careful examination reveals that the peak $2\theta = 44.72^\circ$ corresponded to the (110) plane of Fe^0 [31], and the broad peak between 15–25° could be associated with the amorphous nature of vinylpyrrolidone and vinylacetate [32]. Moreover, the relative intensity of the peak $2\theta = 44.72^\circ$ decreased with the decrease of Fe^{3+} concentration, which may be related to the decreased crystallinity or disturbance from the copolymer on iron surface [33]. Fig. S1 (F) shows an electron diffraction pattern of the area close to the center of PVV/NZVI (2:1), which clearly indicates the presence of vague diffuse rings, and all the diffraction rings from the inside to the surface in SAED pattern could be assigned as α -Fe phase (JCPDS 65-4899) with (110) and (200) planes [34]. However, there was a notable absence of perfect diffuse rings in SAED, indicating the formation of poorly crystalline particles because of being encapsulated in the vesicles. This result also suggests that NZVI particles were well encapsulated in the vesicles.

The FTIR spectra for pure copolymer and PVV/NZVI with different molar ratios of $-\text{COOC}-$ to Fe^{3+} were shown in Fig. S3. Here, the main absorption bands were associated with C–H stretching at 2958 cm^{-1} , C–H bending at 1425 cm^{-1} and 1373 cm^{-1} for poly(1-vinylpyrrolidone-co-vinylacetate) [35], C=O group at 1738 cm^{-1} for vinylacetate and C=O at 1660 cm^{-1} for vinylpyrrolidone [36]. Additionally, the peak at 3448 cm^{-1} could be assigned to O–H stretching of free water [37]. It is clear that the bands for the groups of the copolymer were weakened in the spectra of PVV/NZVI. A small shift from 1660 cm^{-1} to 1655 cm^{-1} was observed for the C=O stretching of vinylpyrrolidone, which might be due to the interaction of NZVI particles with the ester groups in vinylpyrrolidone. Besides, the peak shift of C=O in vinylacetate from 1738 cm^{-1} to 1725 cm^{-1} was more significant as

compared with that in vinylpyrrolidone. Therefore, it is appropriate to state that interaction of NZVI with ester groups of vinylacetate is more favorable, which is helpful to stabilize the NZVI particles in the vesicles.

3.2. Structure and morphology of the NZVI in vesicles

Taking into account the results of synthesis optimization and characterization, PVV/NZVI (2:1) was used to obtain representative NZVI in vesicles to investigate nanostructure and morphology of the NZVI in vesicles. TEM and SEM-EDX images of NZVI in vesicles were shown in Fig. 2. As shown in Fig. 2(A) and (B), all of the as-prepared vesicles before and after Fe^0 formation were well-separated from each other and uniform in shape, which indicates that the dispersibility of the NZVI in vesicles was very good. However, it can be seen from Fig. 2(D) that the bare NZVI particles tended to aggregate together due to magnetic property of the particles. From the location of the NZVI particles observed by TEM, it is suggested that the NZVI particles were mostly anchored to the cavities of the vesicles with an average diameter of about 50 nm. Average diameter of the as-prepared vesicles before and after Fe^0 formation was calculated to be 93.7 and 86.7 nm, respectively.

Furthermore, the cavity and wall structure of the vesicles before and after Fe^0 formation was visible in the TEM images, and the cavity and wall of vesicle all appeared darker after Fe^0 formation, indicating Fe^0 distribution in the vesicles. There is a faint gray layer between the cavity and wall, which could be attributed to the formation of bilayer membrane of the vesicles. These bilayer membranes, with around 20 nm in width, resulted in the interspace inside the individual entity and the enhancement of dispersion of the NZVI in vesicles. NZVI distribution within vesicles was also detected by SEM-EDX mapping analysis of the samples dropped on a TEM copper grid. Fig. 2(C) and (D) shows the SEM images of NZVI in vesicles, bare NZVI and their corresponding EDX elemental mapping (inset), respectively. It can be seen clearly from Fig. 2(C) that in the presence of PVV, Fe elements were uniformly dispersed through the whole vesicle. On the contrary, in the absence of PVV, Fe elements were located in a single spherical aggregate of NZVI (Fig. 2(D)). The EDX mapping results presented here for NZVI in vesicles not only verified that the dispersion of NZVI particles in the vesicle can be well controlled in the presence of PVV, but also indicated that Fe particles were located mainly in the cavities of the vesicles, and only a small number of them were outside the whole vesicles.

The intensity-size distribution of the vesicles before and after Fe^0 formation was measured by DLS. It can be seen from Fig. S4 that the size of spherical vesicles before and after Fe^0 formation exhibited narrow distribution with particle dispersion index of 0.196 and 0.332, and the corresponding average hydrodynamic diameter of 96.2 and 84.3 nm respectively, which were close to the values observed by TEM (93.7, 86.7 nm).

3.3. Effect of the vesicles on the reactivity of NZVI particles

To evaluate the effect of vesicles on the reactivity of NZVI particles, the removal efficiency of Cr(VI) by various iron sources was investigated and the results were depicted in Fig. 3 as a function of time. It was shown that in the presence of pure copolymer, no measurable Cr (VI) loss was observed, indicating that pure copolymer had no contribution to the removal of Cr(VI) from water over the reaction course. However, the residual concentration of Cr(VI) dramatically decreased when PVV/NZVI particles were introduced into the aqueous solution. For example, more than 95.4% of Cr(VI) was removed by PVV/NZVI (2:1) only within 1 min, comparatively, the removal efficiency of Cr(VI) by the bare NZVI and commercial micro-scale Fe powder was only 36.1% and 0.8%, respectively, under similar conditions. Furthermore, when the molar ratios of $-\text{COOC}-$ to Fe^{3+} was equal to and greater than 2:1, such as PVV/NZVI (8:1), PVV/NZVI (4:1) and PVV/NZVI (2:1), the synthesized NZVI in vesicles all have a higher removal

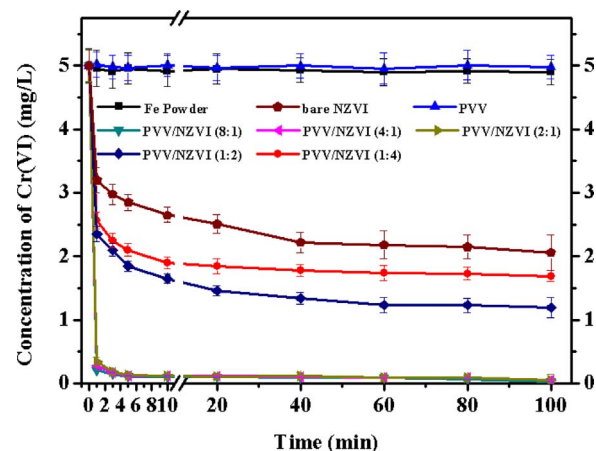


Fig. 3. Removal of Cr(VI) by seven iron sources and pure polymer (iron dose, 0.050 g L⁻¹; stirring speed, 180 rpm; initial concentration, 5 mg L⁻¹; initial pH, 5.6; temperature, 25 °C).

efficiency. However, there was a significant decrease in the Cr(VI) removal by NZVI in vesicles as the molar ratio of $-\text{COOC}-$ to Fe^{3+} was smaller than 2:1. This result can be explained from the fact that NZVI particles tend to agglomerate into larger ones at high Fe^{3+} concentration (Fig. S1). The superior removal characteristics of PVV/NZVI (2:1) over the bare NZVI may be ascribed to the good dispersion of the former, which indicates large surface area and more reactive sites for the reaction, thus enhancing the reactivity of NZVI toward contaminants. At the same time, this result suggests that vesicles can be well used as ideal template for the growth of metal and prevent metal nanoparticles from aggregation [38].

To confirm the Cr(VI) reduction by PVV/NZVI (2:1) and bare NZVI, XPS analyses were performed and the results were shown in Fig. S5. It is clear that four Cr photoelectron peaks were observed after the reduction by the bare NZVI, where the Cr 2p_{3/2} peak at 576.6 eV and the Cr 2p_{1/2} peak at 586.8 eV were consistent with the reported values for Cr (III), and the peaks at 577.4 eV and 589.3 eV were assigned to Cr(VI) [39]. However, after the reduction by PVV/NZVI, only two Cr photoelectron peaks were observed (at 576.4 eV and 586.8 eV), which were comparable to the reported values for Cr(III) [40]. These XPS results suggest that only Cr(III) existed after the reaction of Cr (VI) by PVV/NZVI (2:1), and the removed Cr(VI) of 99.4% (see Fig. 3) was almost completely reduced into Cr(III). Combined with the measurements of removal efficiency of Cr(VI) and total chromium concentration in the solution, it was found that only 41.8% of the removed Cr(VI) was reduced to Cr(III) by bare NZVI under the same conditions (see S6 for details).

In order to investigate pH variation during the reaction and the effect of PVV addition on solution pH values, the variation of pH during the reactions of Cr(VI) with PVV/NZVI (2:1), bare NZVI and PVV was determined at initial pH = 5.6 and the results were presented in Fig. S6. As shown in this figure, the PVV addition has almost no effect on solution pH during the reactions. The solution pH with PVV/NZVI (2:1) first increased from pH 5.6 to pH 8.0, and then reached a plateau with increasing reaction time, and the trend of pH change was similar to that with the bare NZVI.

However, it is known that Cr(VI) reduction by Fe^0 ($2\text{CrO}_4^{2-} + 3\text{Fe}^0 + 10\text{H}^+ \rightarrow 2\text{Cr(OH)}_3 + 3\text{Fe}^{2+} + 2\text{H}_2\text{O}$) leads to the production of OH^- and thus the increase of solution pH [41]. Due to the much higher removal efficiency of Cr(VI) by PVV coated NZVI particles than by the bare NZVI, the use of PVV/NZVI (2:1) resulted in bigger pH change (from pH 5.6 to pH 8.0) than the use of the bare NZVI (from pH 5.6 to pH 7.0). These results are in agreement with those of a recently published work on Cr(VI) removal from aqueous solution using ZVI nanoparticles supported on mesoporous silica [42].

Even more significant is that when dried PVV/NZVI (2:1) particles were added into aqueous solution for less than 1 min, the vesicles could be ruptured, and fresh NZVI particles would be easily released in water, which has been confirmed by the following experiments. Fig. S7 shows the morphology of PVV/NZVI (2:1) in aqueous solution. Compared with the TEM images of PVV/NZVI (2:1) in water/THF (Fig. 2), the vesicles almost disappeared in aqueous solution, and an organic layer and many small particles were observed, which suggests that the vesicles were broken and the NZVI particles were well released from the vesicles. Fig. S7 (B) reveals that NZVI particles released from vesicles had a diameter of 20–30 nm. This indicates that block copolymer plays an essential role in controlling the particle size distribution of NZVI. Besides, in the high-resolution transmission electron microscopy (HRTEM) image of Fig. S7 (C), the lattice fringe spacing is clearly visualized, which was measured at 0.205 nm within the typical range of the interplanar spacing of α -Fe (110). All the diffraction rings in the SAED pattern could be indexed as α -Fe phase (JCPDS 65-4899) with (110), (200) and (222) planes from the inside to the surface [34]. There is a notable existence of a lattice fringe and perfect diffuse rings in SAED pattern, suggesting that the NZVI particle was perfectly crystalline. Therefore, these results confirm that fresh NZVI was easily released from vesicles in water.

3.4. Effect of the vesicles on the stability of NZVI particles

Because NZVI can be easily oxidized and become deactivated in the air, the stability of NZVI in vesicles under air exposure is an important concern for their practical application. XRD spectra of the NZVI in vesicles and the bare NZVI particles were depicted in Fig. 4. It was shown that for the NZVI in vesicles, the signals of Fe^0 (peak at 44.72°) were detected obviously and no significant variation was observed in XRD after air exposure for 90 days, implying that fewer oxides could be formed or the formed iron oxide was poorly crystalline. However, for the bare NZVI sample, a weak signal of the iron oxide shell (peak at 36°) appeared after air exposure for 5 days. Notably, the characteristic peaks of Fe_2O_3 at 23, 27 and 36° (JCPDS No. 47-1409) were obviously observed after air exposure for 90 days. Compared with the NZVI in vesicles, the peak intensity at 44.72° of the bare NZVI particles decreased significantly after air exposure for 90 days, because the bare NZVI is very reactive and even ignites when exposure to air [43]. XRD analysis indicates that vinylacetate as the hydrophobic block of the vesicles could inhibit the interaction of NZVI with O_2 or H_2O when exposure to air. Thus, encapsulation within vesicles is an effective approach to stabilizing nanoparticles [44].

The high stability of NZVI in vesicles can be further confirmed by a comparative study of Cr(VI) removal by the bare NZVI and the NZVI in

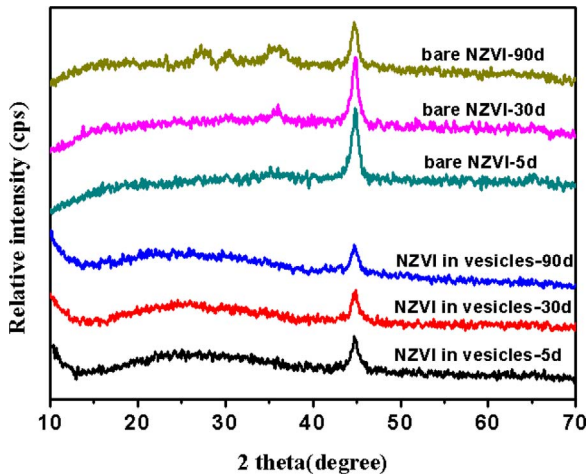


Fig. 4. XRD patterns of the bare NZVI and the NZVI in vesicles at different air exposure times (5 d, 30 d, 90 d).

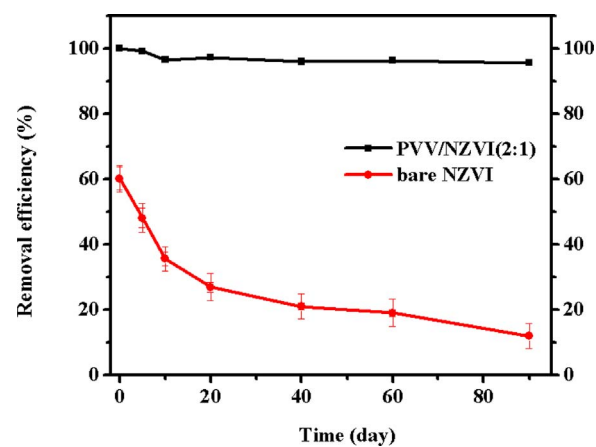


Fig. 5. Cr(VI) removal by the bare NZVI and the NZVI in vesicles under air exposure for 90 days (iron dose, 0.050 g L^{-1} ; stirring speed, 180 rpm; initial concentration, 5 mg L^{-1} ; initial pH, 5.6; temperature, 25°C).

vesicles which were exposed in the air for 90 days. It is noted from Fig. 5 that only 4.4% decrease was observed for the removal efficiency by using the NZVI in vesicles, while remarkable decrease (88%) was confirmed by using the bare NZVI particles. These results suggest that the bare NZVI particles were significantly oxidized to iron oxide/hydroxide, and the vesicles played a critical role in keeping the high stability of NZVI in vesicles in the air. This point is very important because it is not necessary to protect the NZVI particles with inert gas in the air, thus greatly enhancing the potential for long-term and commercial utilization of the NZVI for pollutant detoxification and other applications.

3.5. Application of NZVI in vesicles for nitrobenzene degradation

In order to evaluate the reactivity of NZVI in vesicles to organic pollutants, nitrobenzene was used as a model pollutant to investigate the performance of NZVI in vesicles for the degradation of the simulated organic wastewater. It was found from Fig. 6 that pure block copolymer had no contribution to the removal of nitrobenzene in water, while the degradation efficiency of nitrobenzene by NZVI in vesicles increased dramatically with reaction time. For example, more than 79.2% of nitrobenzene was removed by NZVI in vesicles just within 1 min, but in the control experiment, the removal percent of nitrobenzene by the bare NZVI was only about 18.3%. As the reaction

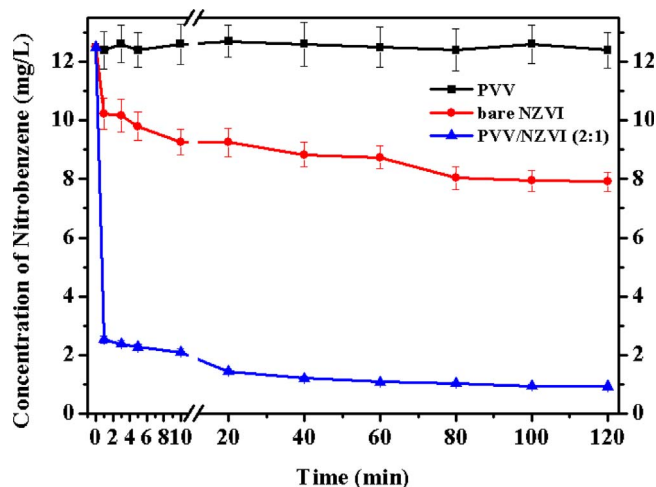


Fig. 6. Removal of nitrobenzene by the NZVI, the bare NZVI and the pure block copolymer (iron dose, 0.050 g L^{-1} ; stirring speed, 180 rpm; initial concentration, 12.5 mg L^{-1} ; pH, 6.0; temperature, 25°C).

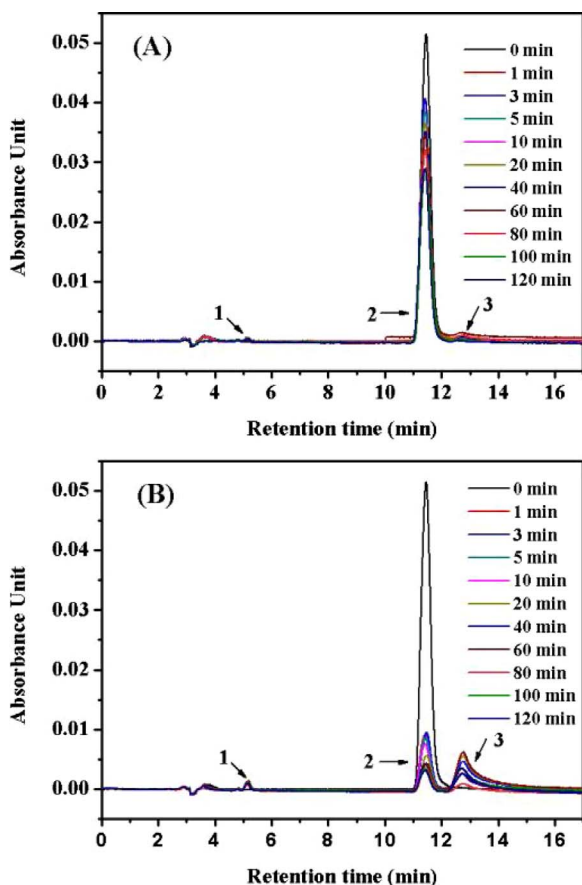


Fig. 7. HPLC of the samples at pre-determined reaction time for bare NZVI (A), NZVI in vesicles (B), 1-aniline, 2-nitrobenzene, and 3-nitrosobenzene.

time was prolonged to 120 min, degradation efficiency of nitrobenzene by NZVI in vesicles and bare NZVI was measured to be 92.6% and 36.7%, respectively. Obviously, the NZVI in vesicles displayed much higher reactivity than the bare NZVI.

Nitrobenzene has the character of low water solubility and strong sorption onto inorganic/mineral surfaces [45]. In order to investigate the degradation process of nitrobenzene, kinetic models were used to fit the experimental data. It is known that the pseudo-first-order and pseudo-second-order models are commonly expressed by Eqs. (1) and (2) [46]:

$$\ln(q_e - q_t) = \ln q_e - k_1 t \quad (1)$$

$$\frac{t}{q_t} = \frac{1}{k_2 q_e^2} + \frac{t}{q_e} \quad (2)$$

In Eq. (1), q_t and q_e are the amounts of nitrobenzene adsorbed per unit mass (mg g^{-1}) at any time (t) and at equilibrium, respectively, and k_1 is the rate constant of first-order adsorption (min^{-1}). In Eq. (2), k_2 is the second order rate constant ($\text{g mg}^{-1} \text{min}^{-1}$). The fitting parameters from the experimental data included in Fig. 7 were shown in Table S1. From the comparison of the correlation coefficients, it is clear that the removal of nitrobenzene by both NZVI in vesicles and bare NZVI could be well described by the pseudo-second order kinetics model. On the other hand, the reaction rate constant k_2 and the amounts of nitrobenzene removed at equilibrium (q_e) by NZVI in vesicles were about 3.0 and 2.5 times that by the bare NZVI at the same conditions. This result also implies that the rate-limiting step may be a chemical sorption.

The reductive transformation of nitrobenzene by the bare NZVI particles and NZVI in vesicles was further investigated by the HPLC analysis of the un-reacted nitrobenzene and various reaction products

during the degradation. It can be seen from Fig. 7 that two products were observed in the degradation reactions of nitrobenzene by both NZVI in vesicles and bare NZVI. Similar HPLC results were also reported for nitrobenzene degradation by NZVI particles in other systems [47]. The final reductive products with the retention time of 5.1 and 12.7 min correspond to aniline (AN) and nitrosobenzene (ArNO), respectively. Based on the observed similarity of HPLC patterns and retention time of the products, it can be assumed that the bare NZVI and NZVI in vesicles degraded nitrobenzene in the similar way, as shown in S10. However, the removal efficiency and reaction rate by NZVI in vesicles are significantly higher than those by the bare NZVI.

4. Conclusions

In this study, novel NZVI in the vesicles of PVV was synthesized in aqueous THF solution, characterized with XRD, FTIR, SEM-EDX, TEM, XPS and DLS techniques, and applied for the degradation of nitrobenzene and Cr(VI) in water for the first time. It was found that particle size, size distribution, structure and morphology of the NZVI particles could be controlled by encapsulation in the vesicles. The as-prepared NZVI in vesicles showed a strong reactivity in the removal of pollutants in water. More than 79.2% of nitrobenzene and 95.4% of Cr (VI) could be degraded by NZVI in vesicles within 1 min, whereas the degradation efficiency by the bare NZVI particles was only 18.3% for nitrobenzene and 36.1% for Cr(VI) under the same conditions. Furthermore, high stability was found for the NZVI in vesicles in the air. For example, even after exposing the dried NZVI in vesicles to the air for 90 days, only 4.4% decrease was observed in the removal efficiency of Cr(VI), while the corresponding decrease was 88% for the bare NZVI particles. These findings indicate that encapsulation in the vesicles is an effective approach to keep the reactivity and stability of the NZVI particles due to the protection of the particles from agglomeration and oxidation. The results reported here may be useful for the design of new nanocontainer for preparation, storage and release of fresh NZVI particles.

Acknowledgements

This work was supported financially from the National Natural Science Foundation of China (No. 21377036), the Key scientific research project of Higher Education of Henan (No. 14B430020), the Project of Henan Science and Technology (No. 142102210456) and the Research Innovation Program for College Graduates of Henan Normal University (No. YL201525).

Appendix A. Supplementary data

Supplementary data associated with this article can be found, in the online version, at <http://dx.doi.org/10.1016/j.apcatb.2017.09.057>.

References

- [1] W.-L. Yan, H.L. Lien, B.E. Koel, W.-X. Zhang, Environ. Sci.: Processes Impacts 15 (2013) 63–77.
- [2] F. Liang, J. Fan, Y.-H. Guo, M.-H. Fan, J.-J. Wang, H.-Q. Yang, Ind. Eng. Chem. 47 (2008) 8550–8554.
- [3] I.H. Yoon, K.W. Kim, S. Bang, M.G. Kim, Appl. Catal. B: Environ. 104 (2011) 185–192.
- [4] S.-L. Xiao, M.-W. Shen, R. Guo, Q.-G. Huang, S.-Y. Wang, X.-Y. Shi, J. Mater. Chem. 20 (2010) 5700–5708.
- [5] S. Giri, M. Bhattacharjee, R. Das, V.K. Gupta, A. Maity, Appl. Catal. B: Environ. 202 (2017) 207–216.
- [6] R.-W. Liang, F.-F. Jing, L.-J. Shen, N. Qin, L. Wu, J. Hazard. Mater. 287 (2015) 364–372.
- [7] S. Luo, T.-T. Lu, L. Peng, J.-H. Shao, Q.-R. Zeng, J.-D. Gu, J. Mater. Chem. 2 (2014) 15463–15472.
- [8] T. Phenrat, N. Saleh, K. Sirk, R.D. Tilton, G.V. Lowry, Environ. Sci. Technol. 41 (2007) 284–290.
- [9] R.L. Johnson, J.T. Nurmi, G.S.O. Brien Johnson, D. Fan, R.L.O. Brien Johnson, Z. Shi, A.J. Salter-Blanc, P.G. Tratnyek, G.V. Lowry, Environ. Sci. Technol. 47

- (2013) 1573–1580.
- [10] H. Dong, I.M.C. Lo, Water Res. 47 (2013) 419–427.
- [11] H. Dong, I.M.C. Lo, Water Res. 47 (2013) 2489–2496.
- [12] Y.-M. Li, W. Cheng, G.-D. Sheng, J.-F. Li, H.-P. Dong, Y. Chen, L.-Z. Zhu, Appl. Catal. B: Environ. 174–175 (2015) 329–335.
- [13] J. Luan, P.-X. Hou, C. Liu, C. Shi, G.-X. Li, H.-M. Cheng, J. Mater. Chem. A 4 (2016) 1191–1194.
- [14] P.D. Mines, J. Byun, Y.-H. Wang, H.A. Patel, H.R. Andersena, C.T. Yavuz, J. Mater. Chem. A 4 (2016) 632–639.
- [15] L.-C. Wang, S.-Q. Ni, C.-L. Guo, Y.-T. Qian, J. Mater. Chem. A 1 (2013) 6379–6387.
- [16] J.-C. Yang, X.-Y. Wang, M.-P. Zhu, J. Hazard. Mater. 264 (2014) 269–277.
- [17] Y.-T. Li, A.E. Smith, B.S. Lokitz, C.L. McCormick, Macromolecules 40 (2007) 8524–8526.
- [18] Y.-Y. Mai, A. Eisenberg, J. Am. Chem. Soc. 132 (2010) 10078–10084.
- [19] S. Klingelöfer, W. Heitz, A. Greiner, S. Oestreich, S.F. Örster, M. Antonietti, J. Am. Chem. Soc. 119 (1997) 10116–10120.
- [20] T.F. Jaramillo, S.H. Baeck, B.R. Cuanya, E.W. McFarland, J. Am. Chem. Soc. 125 (2003) 7148–7149.
- [21] J. Lin, S.-J. Wang, P. Huang, Z. Wang, S.-H. Chen, G. Niu, W.-W. Li, J. He, D.-X. Cui, G.-M. Lu, X.-Y. Chen, Z.-H. Nie, Nano 7 (2013) 5320–5329.
- [22] Z. Jiang, S. Zhang, B. Pan, W. Wang, X. Wang, L. Lv, W. Zhang, Q. Zhang, J. Hazard. Mater. 233 (2012) 1–6.
- [23] X. Wang, C. Chen, H. Liu, J. Ma, Water Res. 42 (2008) 4656–4664.
- [24] M. Gheju, A. Iovi, I. Balciu, J. Hazard. Mater. 153 (2008) 655–662.
- [25] Y.-Y. Mai, A. Eisenberg, Chem. Soc. Rev. 41 (2012) 5969–5985.
- [26] Y.-S. Yu, L.-F. Zhang, A. Eisenberg, Macromolecules 31 (1998) 1144–1154.
- [27] R. Nair, N. Nyamweya, S.G. Önen, L.J. Martínez-Miranda, S.W. Hoag, Int. J. Pharm. 225 (2001) 83–96.
- [28] N. Deslandes, V. Bellenger, F. Jaffiol, J. Verdu, J. Appl. Polym. Sci. 69 (1998) 2663–2671.
- [29] D.R. Lide, CRC Handbook of Chemistry and Physics, 78th Ed. CRC Press : New York, 1997–1998. p 6–139.
- [30] Y.-L. Wang, P.H.C. Camargo, S.E. Skrabalak, H.-C. Gu, Y.-N. Xia, Langmuir 24 (2008) 12042–12046.
- [31] B.-W. Zhu, T.T. Lim, J. Feng, Environ. Sci. Technol. 42 (2008) 4513–4519.
- [32] P.-G. Liu, K.-C. Gong, P. Xiao, M. Xiao, J. Mater. Chem. 10 (2000) 933–935.
- [33] L. Zhou, T.L. Thanh, J. Gong, J.H. Kim, E.J. Kim, Y.-S. Chang, Chemosphere 104 (2014) 155–161.
- [34] Q. Wang, S. Lee, H.C. Choi, J. Phys. Chem. C 114 (2010) 2027–2033.
- [35] C.M. Zaccaron, R.V.B. Oliveira, M. Guiotoku, A.T.N. Pires, V. Soldi, Polym. Degrad. Stab. 90 (2005) 21–27.
- [36] Z.A. Worku, J. Aarts, A. Singh, G.V. Mooter, Mol. Pharm. 11 (2014) 1094–1101.
- [37] S.-L. Xiao, S.-Q. Wu, M.-W. Shen, R. Guo, Q.-G. Huang, S.-Y. Wang, X.-Y. Shi, ACS Appl. Mater. Interfaces 12 (2009) 2848–2855.
- [38] Y. Zhou, H.-C. Zeng, J. Am. Chem. Soc. 136 (2014) 13805–13817.
- [39] J.-J. Du, J.-S. Lu, Q. Wu, C.-Y. Jing, J. Hazard. Mater. 215–216 (2012) 152–158.
- [40] X.-Y. Li, L.-H. Ai, J. Jiang, J. Chem. Eng. 288 (2016) 789–797.
- [41] M.J. Alowitz, M.M. Scherer, Environ. Sci. Technol. 36 (2002) 299–306.
- [42] E. Petala, K. Dimos, A. Douvalis, T. Bakas, J. Tucek, R. Zboril, M.A. Karakassides, J. Hazard. Mater. 261 (2013) 295–306.
- [43] Z.-M. Jiang, L. Lv, W.-M. Zhang, Water Res. 45 (2011) 2191–2198.
- [44] J. Wu, A. Eisenberg, J. Am. Chem. Soc. 128 (2006) 2880–2884.
- [45] H.-R. Wang, B. Kim, S.L. Wunder, Environ. Sci. Technol. 49 (2015) 529–536.
- [46] P.-X. Wu, S.-Z. Li, L.-T. Ju, N.-W. Zhu, J.-H. Wu, P. Li, Z. Dang, J. Hazard. Mater. 219 (2012) 283–288.
- [47] X.-F. Ling, J.-S. Li, W. Zhu, Y.-Y. Zhu, X.-Y. Sun, J.-Y. Shen, W.-Q. Han, L.-J. Wang, Chemosphere 87 (2012) 655–660.